Supporting Information

Scalable faceted voids with luminescence enhanced edges in WS_2 monolayers

Pawan Kumar[1], Dipanwita Chatterjee[2], Takuya Maeda[3], Ahin Roy[2,3], Kenji Kaneko[3] and Viswanath Balakrishnan[1]*

[1]School of Engineering, Indian Institute of Technology Mandi, Kamand, H.P., 175005, India.
[2]Material Research Center, Indian Institute of Science, Bengaluru-560012, India.
[3]Department of Materials Science and Engineering, Kyushu University, 744 Motooka, Nishi-ku, Fukuoka, Japan 819-0395.

*Corresponding: viswa@iitmandi.ac.in

Sample preparation and CVD Growth:

Typically, we have taken specific amount of WO_3 nanorod (Hydrothermal based synthesis) and ultra-sonicated with deionized water that uniformly deposited on SiO_2/Si substrate and placed it at center (heating zone-1) of quartz tube furnace. Before the deposition of WO_3 nanorod, SiO_2/Si substrate was cleaned by ultrasonication with Acetone, Isopropyl alcohol followed by Piranha solution (3:1 ratio of H_2SO_4 & H_2O_2) treatment for 3 hours. A boat containing ~400 mg Sulfur powder has been placed on heating zone-2 of same tube furnace such that the sulfurization of WO_3 nanorod can be achieved near growth temperature. We have adopted two different ramping rates of 20°C/min. up to 500°C and 10°C/min. to reach the final reaction temperature. After growth of monolayer, sample is cooled down to room temperature using natural atmospheric environment.

***In-situ* CVD annealing:**

In-situ CVD process has been done by continued extended growth time, by keeping all parameters constant. On extending the growth time, due to W-precursor reductions at the local reaction zone lead to formation of defects at high reaction temperature. Defect generated into monolayer crystal lead to further formation of faceted voids with ultra-slow process of void reconstructions. During growth, annealing for extended time results the larger areal size of voids which geometrically cover the overall size of parent crystals.

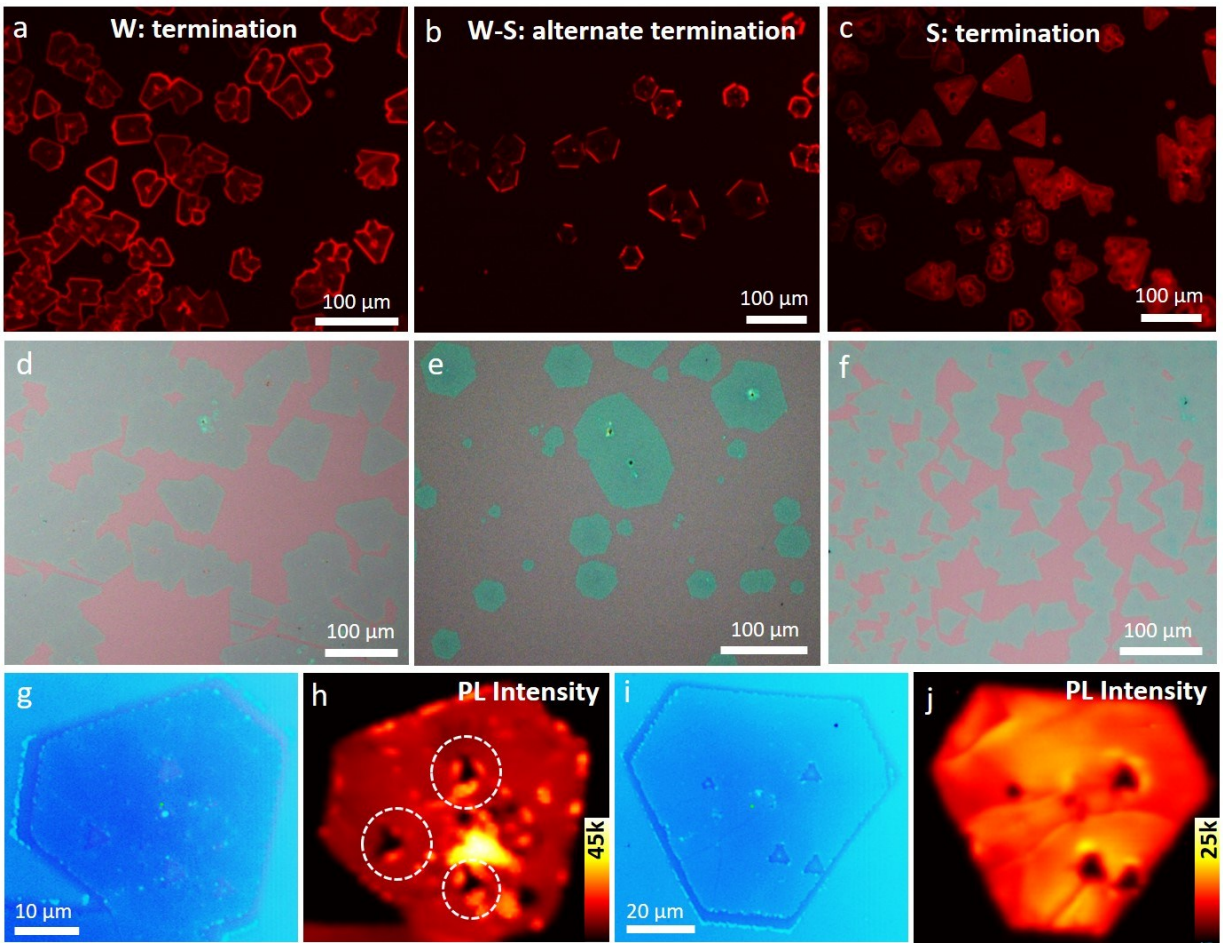

Figure S1: Different atomic edge terminated (a-c) monolayer WS_2 has been captured using fluorescence microscope imaging. The corresponding VLM images has been shown in figure (d-f). PL intensity mapping for two different types of terminated edges (voids) as shown, alternate W-S termination (g-h) and only S-termination (i-j) respectively.

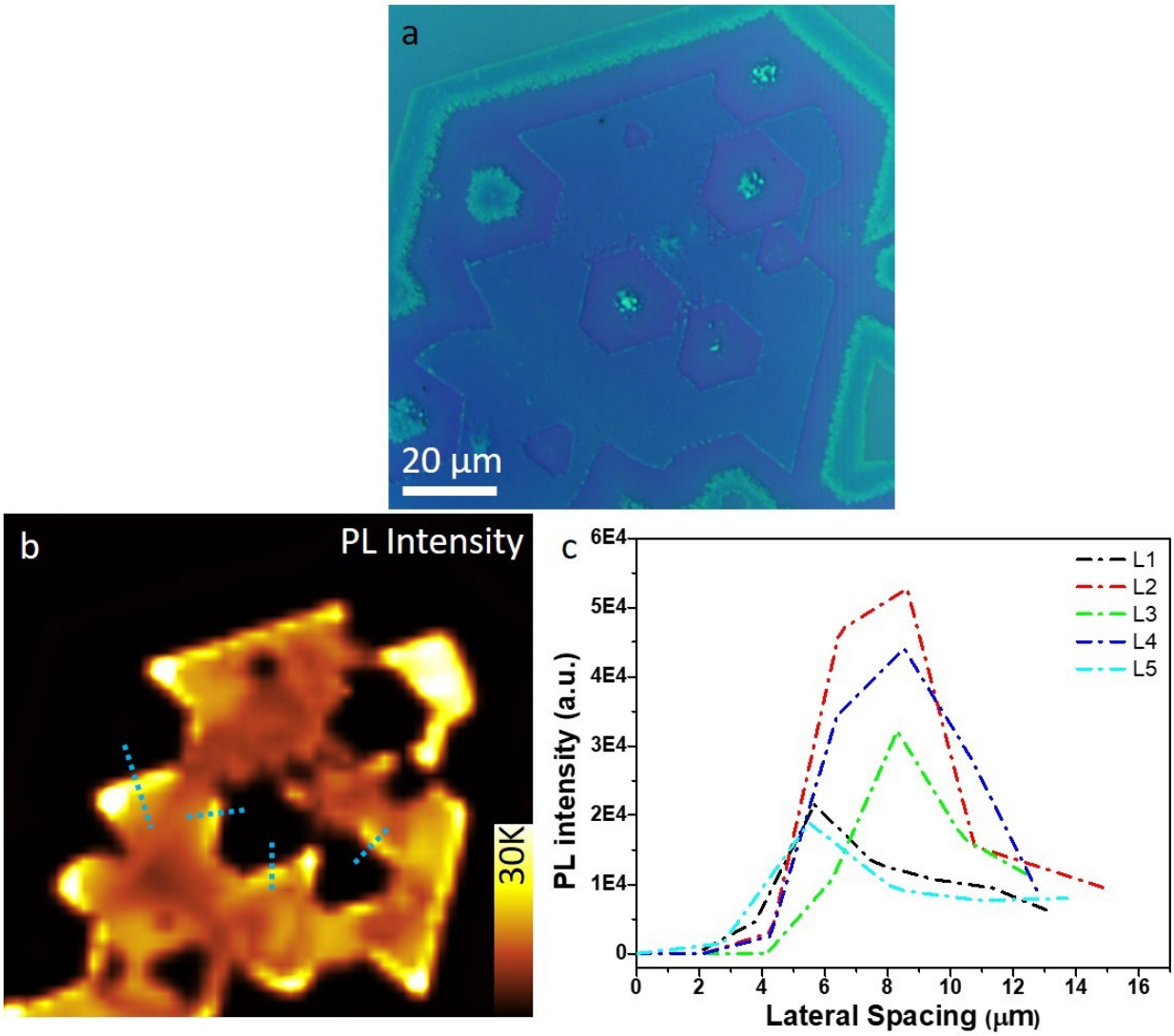

Figure S2: Visible light microscope image (a) of large size faceted voids inside the monolayer WS_2 with corresponding (b) PL intensity mapping where we can clearly see the alternate edges are having enhanced PL intensity. (c) Numbers of PL line profile has been drawn on different void facets where the enhancement can be seen in respect of bare monolayer region.

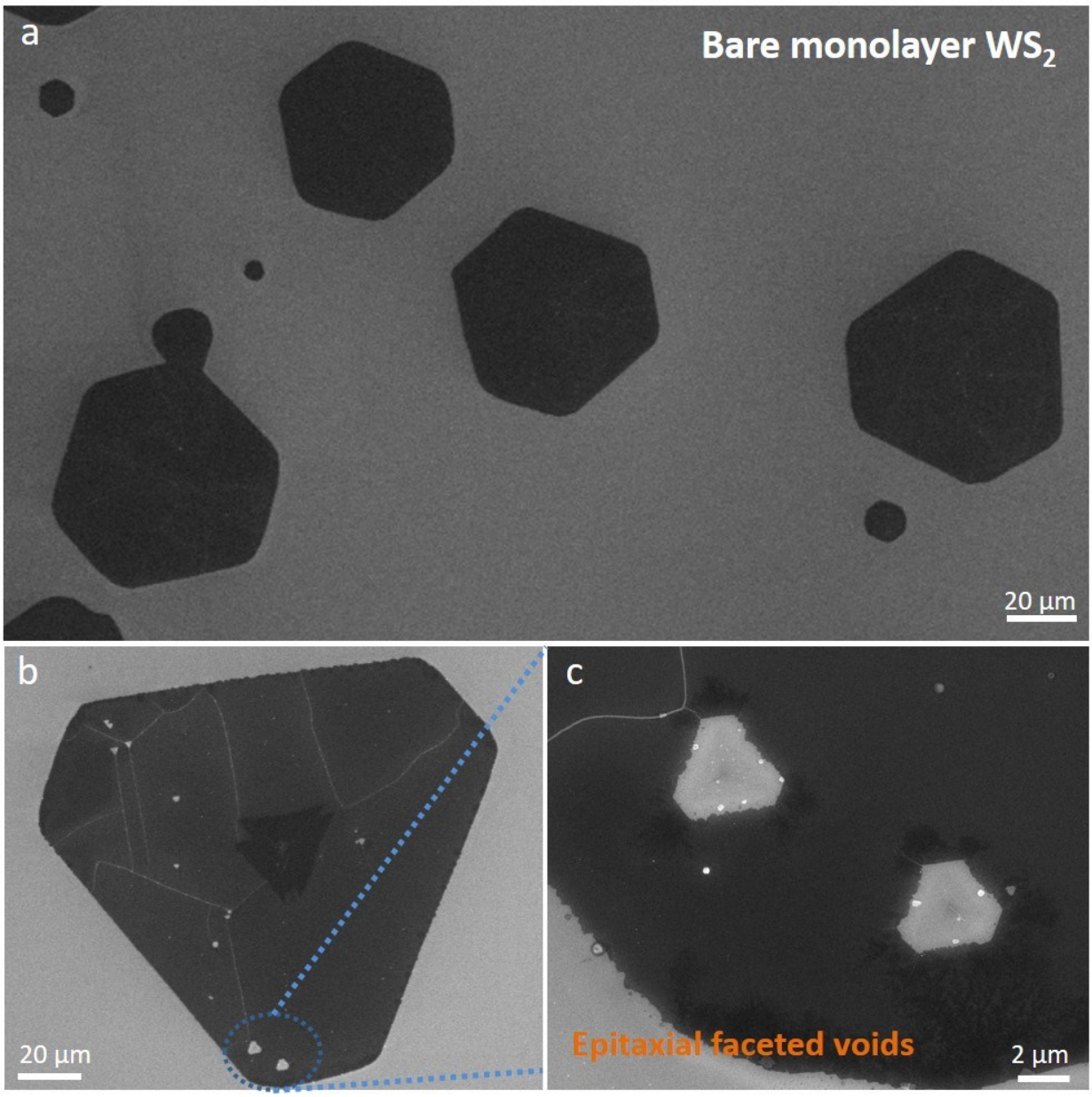

Figure S3: Epitaxial nature of void formation in monolayer WS_2 as shown using FESEM imaging, (a) As grown monolayers and (b-c) after formation of faceted voids with epitaxial nature.

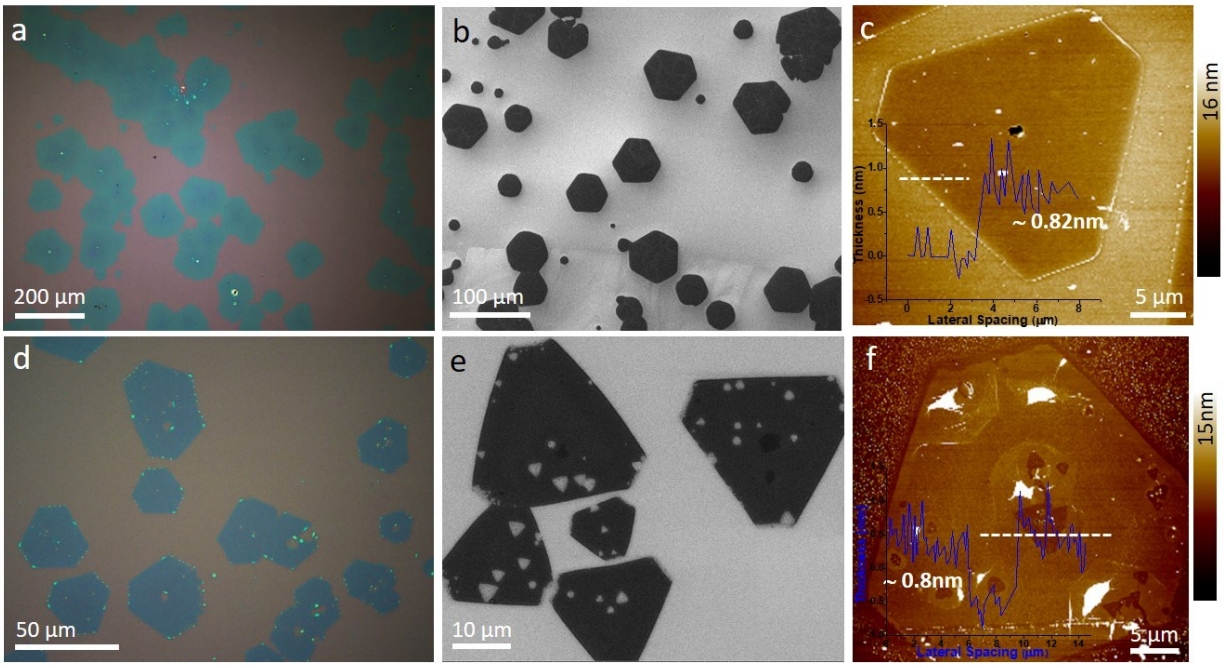

Figure S4: Large area, single domain, 2D monolayer WS_2 grown using APCVD. As grown WS_2 (a-c) and WS_2 monolayer with faceted voids (d-f) are characterized by visible light, scanning electron and atomic force microscope imaging.

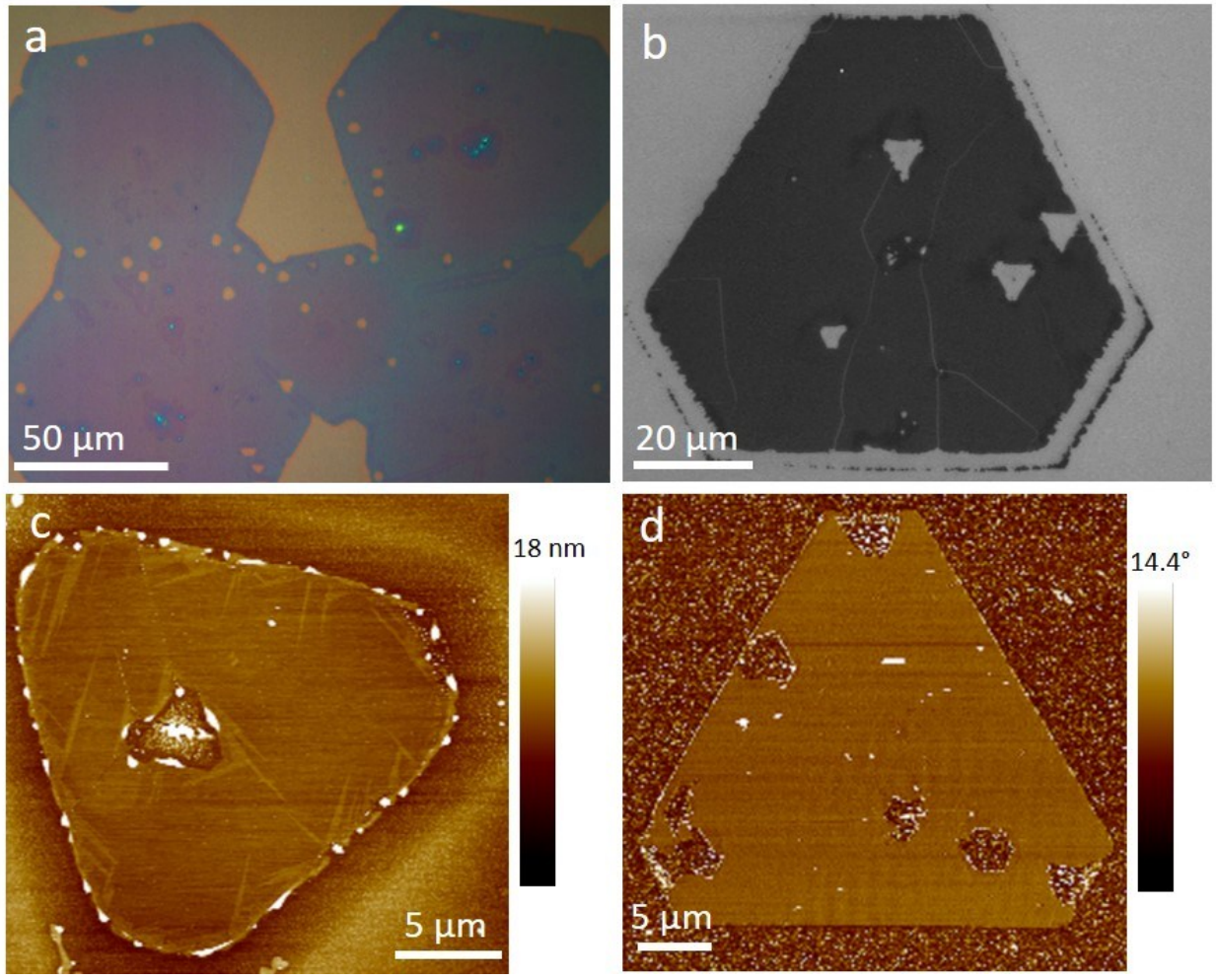

Figure S5: Microscopic observations of faceted voids forming inside the single crystalline monolayer WS_2 domains after dynamic reconstruction during CVD growth. VLM image (a), FESEM image (b) and AFM height as well as phase images (c, d) has been presented to show the nature of faceted voids

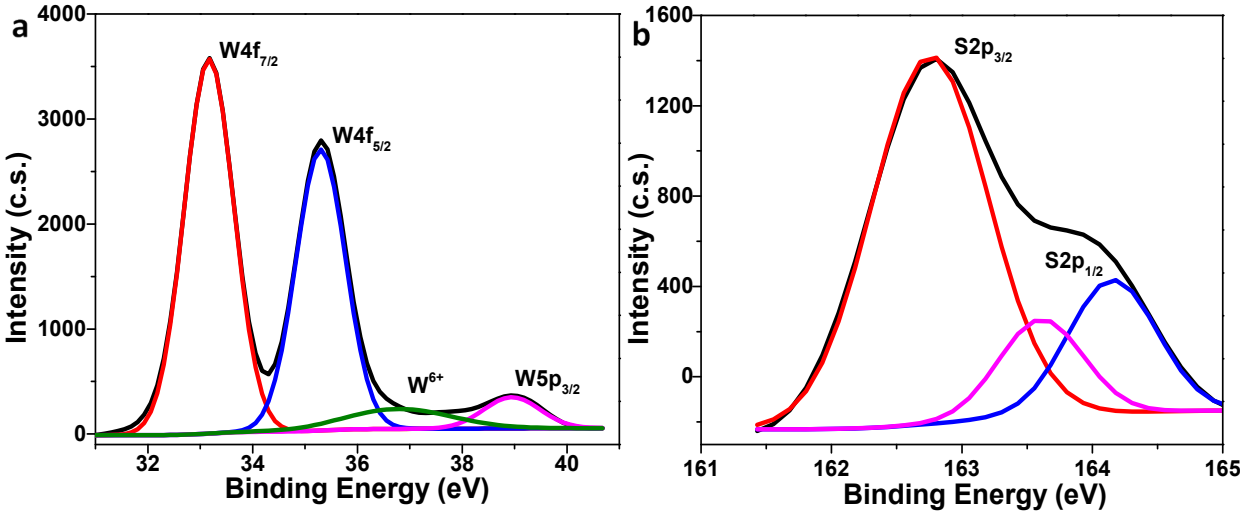

Figure S6: XPS spectra for the monolayer WS_2 having faceted voids, de-convoluted peaks for (a) W^{4+} and W^{6+}, as well as (b) S2p.

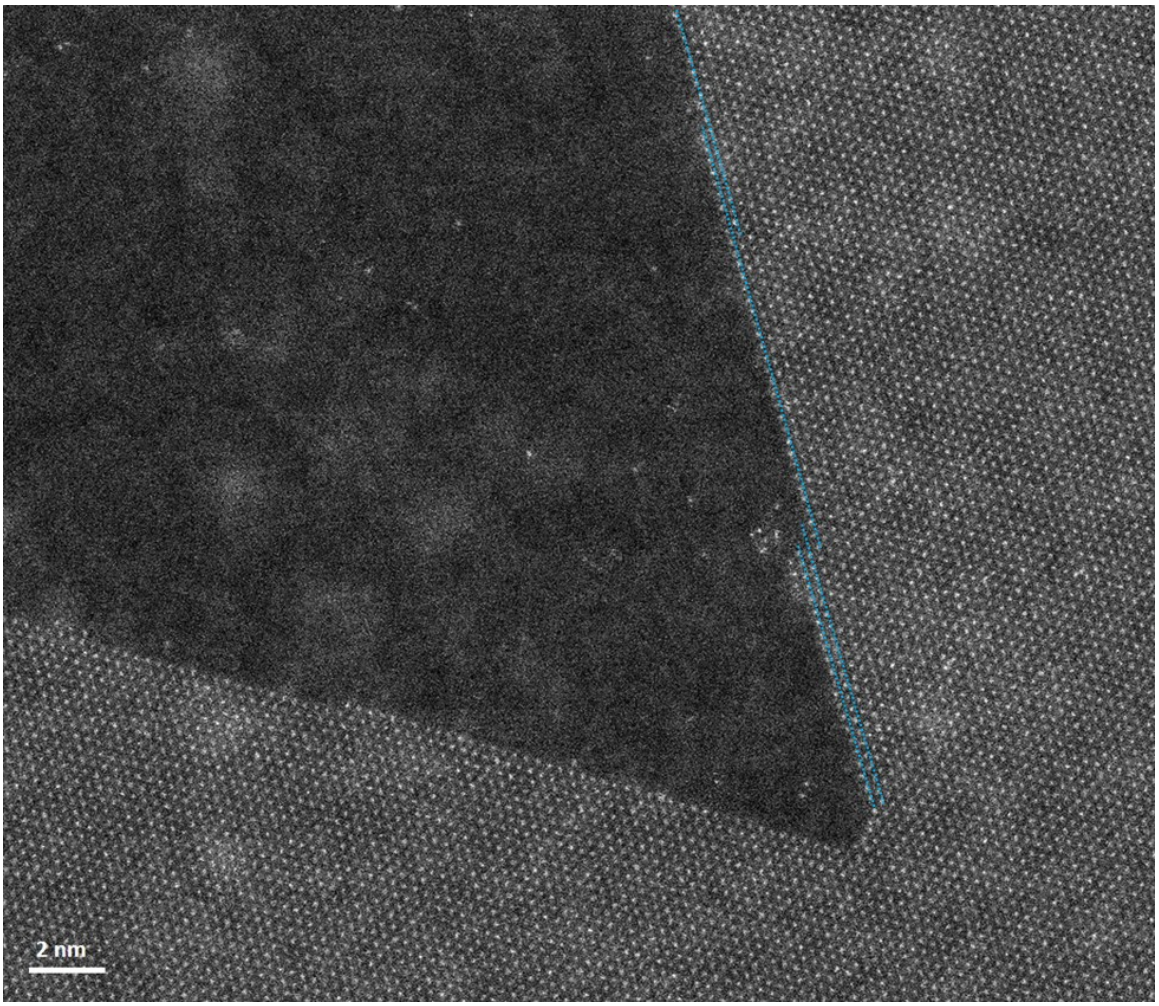

Figure S7: STEM HAADF image for faceted void inside the WS_2 crystal having direct visualization of atomic step formation after slow continuum atom removal process inside the available void in verge of electron beam irradiation.

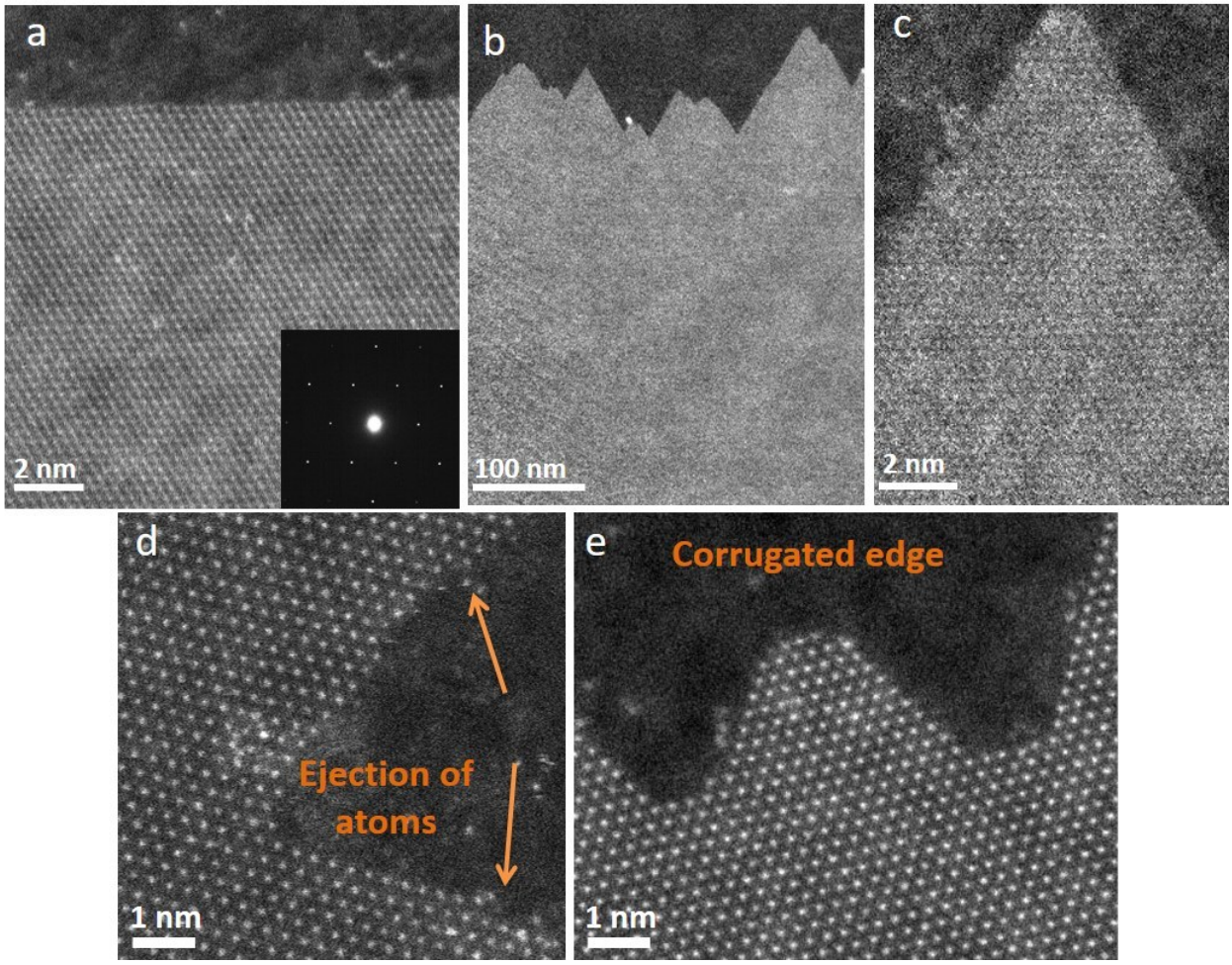

Figure S8: (a) ADF-STEM imaging of single domain 2D monolayer WS_2 transferred on TEM grid with SAED pattern (inset) shows hexagonal symmetry. (b, c) STEM imaging show the outer edges which also formed in zig-zag manner results by void formation. (c, d) AC-STEM images show the ejection of atoms from terrace terminated atomic steps inside the voids and corrugated outer edge of flake after void formation respectively.

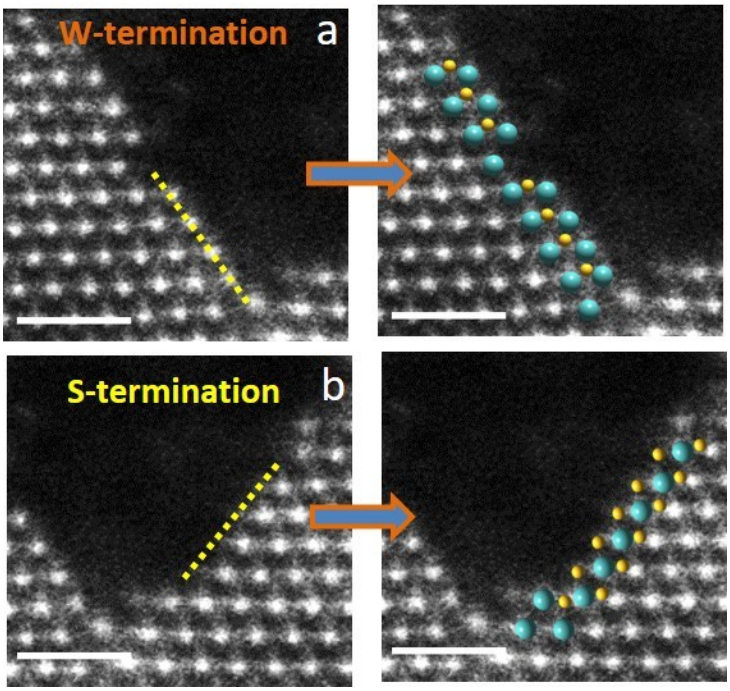

Figure S9: Different edge-termination (W and S) of the faceted void with corresponding stick-ball diagram observed using AC-STEM HAADF imaging.

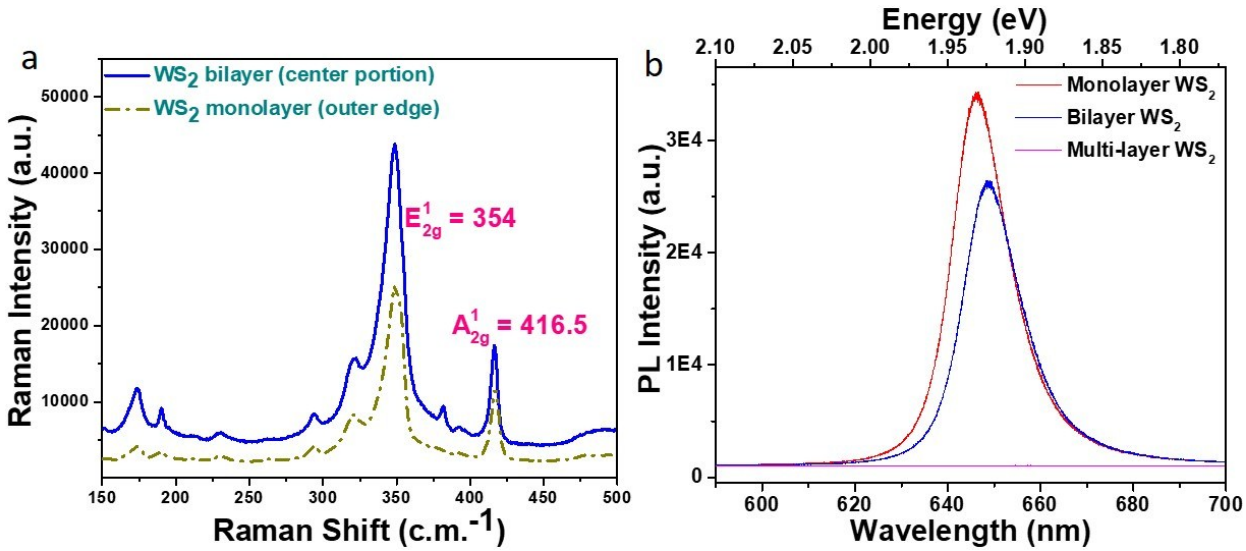

Figure S10: (a) Raman and (b) PL characteristic curves for mono and bilayer WS_2 which gives comparative changes for their vibrational modes as well as emissive peaks.

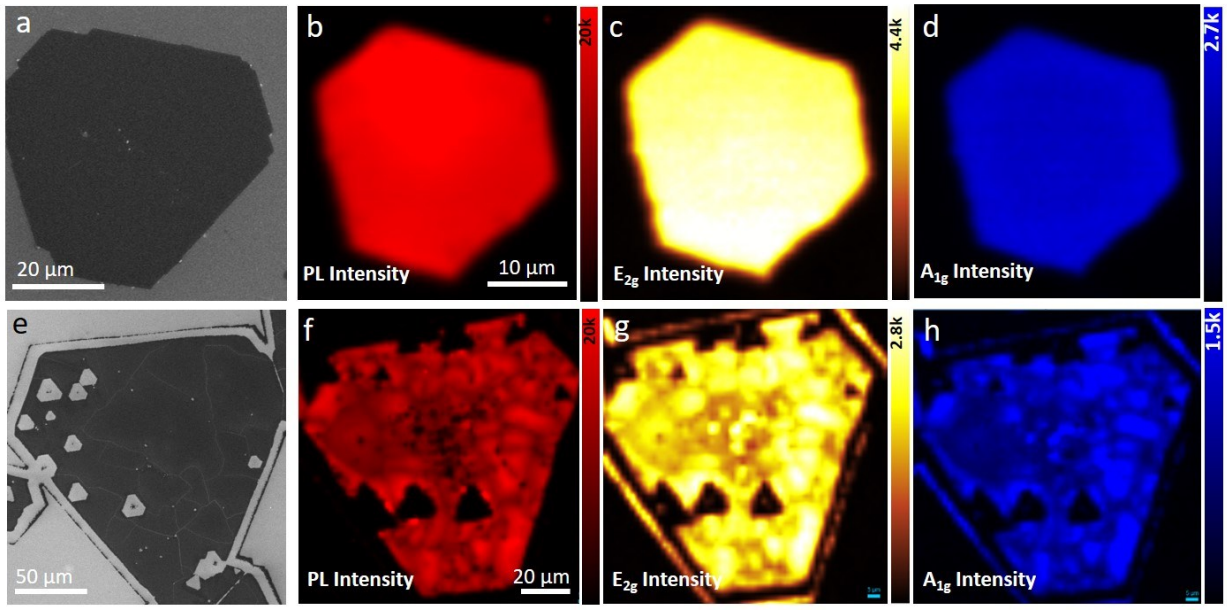

Figure S11: Large area, single domain 2D monolayer WS_2 grown using CVD. As grown WS_2 (a-d) and WS_2 monolayer with faceted voids (e-h) are characterized by secondary electron imaging, PL mapping and Raman mapping respectively. Scale bar shown in (b) and (f) are same for(c-d) and (g-h) respectively. The presented monolayer flakes is having S-termination only such that it has no any enhanced edges before as well after void formation.

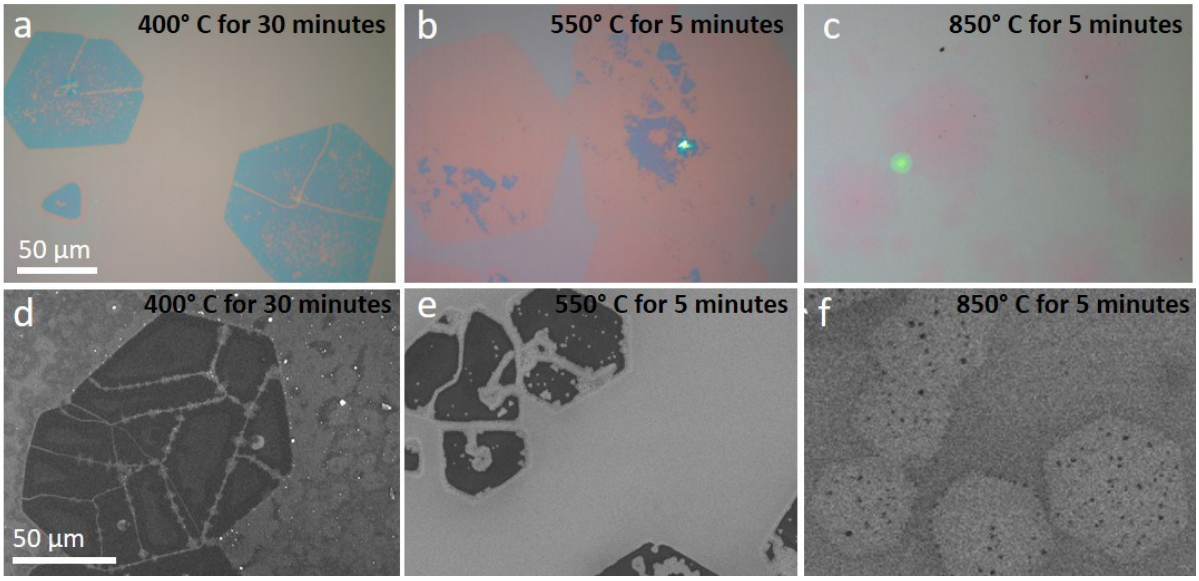

Figure S12: *Ex-situ* post growth annealing of monolayer WS_2 at different temperatures carried out in Ar+H_2 atmosphere (Ar+H_2 = 95+5%). Figure (a-c) representing the VLM image for void formation with increased temperature and corresponding Figure (d-f) FESEM images for same environment. Scale bar is same for (a-c) and (d-f) respectively.

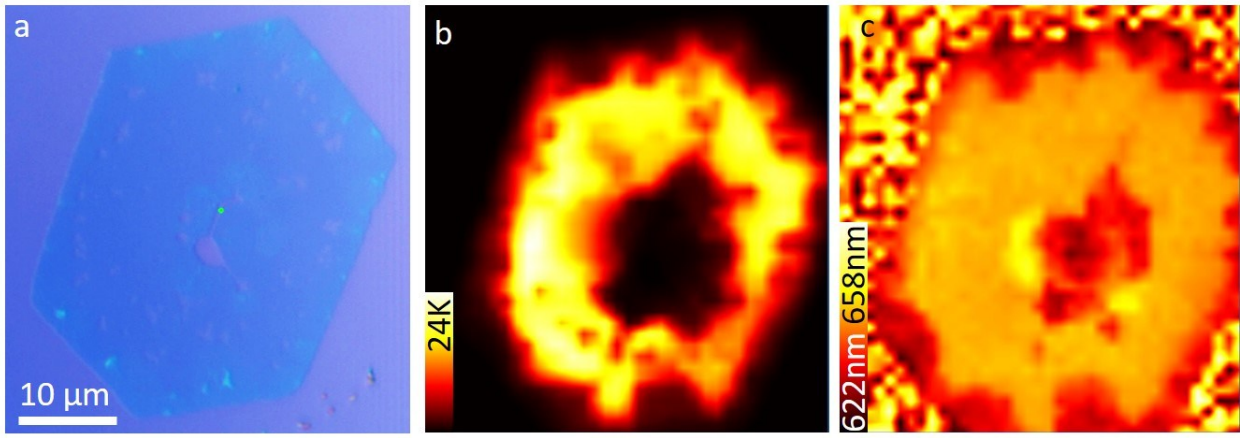

Figure S13: VLM image (a) and corresponding spatially resolved PL intensity (b) and position (c) mapping for monolayer WS_2 which is post-growth annealed at 450°C in $Ar+H_2$ environment.

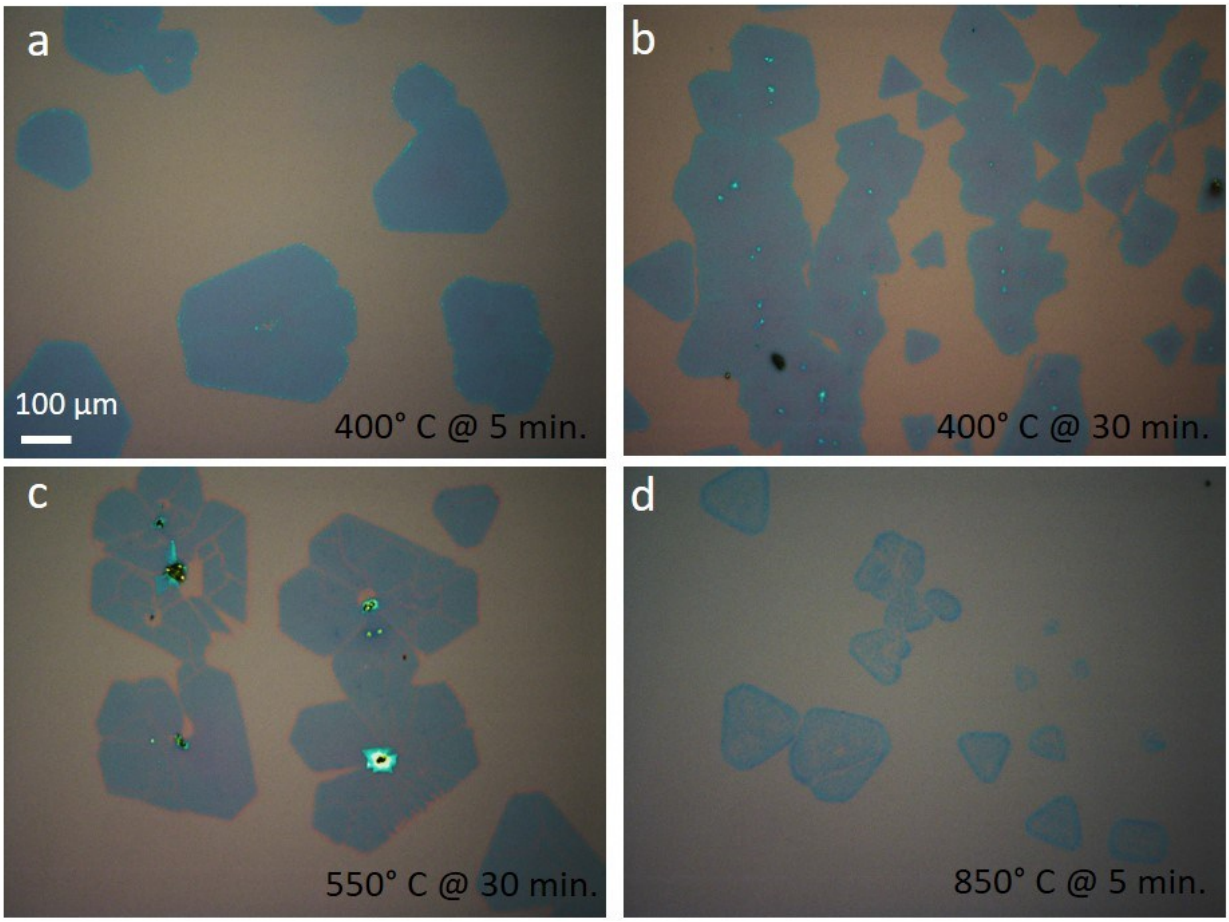

Figure S14: *Ex-situ* post growth thermal treatment on monolayer WS_2 at different temperatures, carried out under high vacuum condition (~10^{-6} mbar).

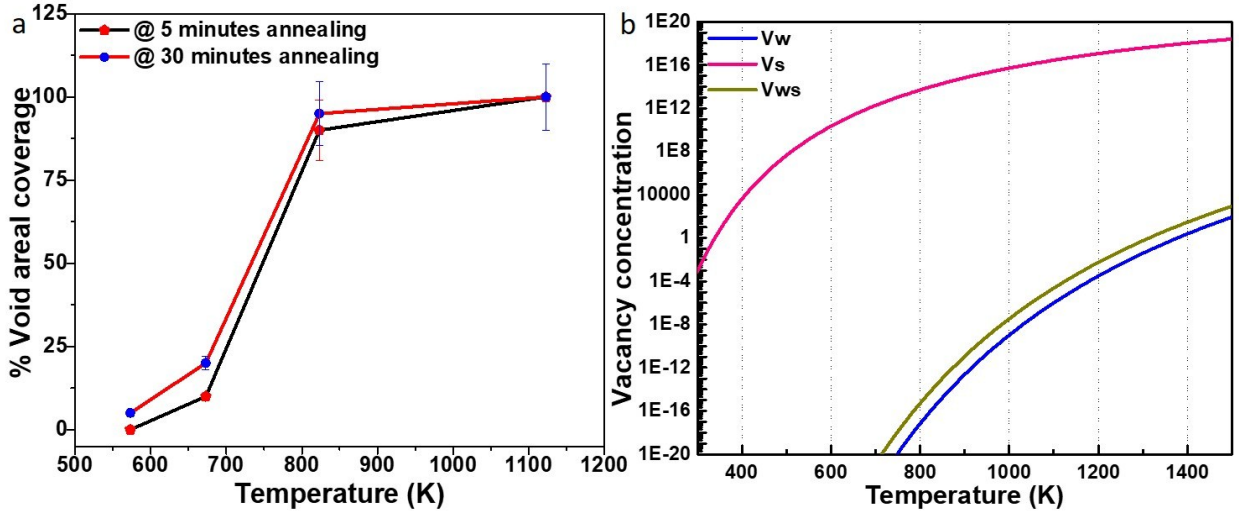

Figure S15: (a) Areal void coverage of voids calculated using FESEM images recorded at different temperatures for two different thermal processing times. (b) Estimated vacancy concentration with increasing temperature in W-rich condition for 2D monolayer WS_2 using formation of energies of different point defects (V_S, V_W, $V_{W\text{-}S}$).